



Thermodynamic and buoyancy force effects of Cu and TiO₂ nanoparticles in engine oil flow over an inclined permeable surface

Raghunath Kodi^{a,*}, Ramachandra Reddy Vaddemani^b, Haribabu Kommaddi^c,
Samad Noeiaghdam^{d,e,*}, Unai Fernandez-Gamiz^f

^a Department of Humanities and Sciences, St. Johns College of Engineering Technology, Yemmiganur 518360, Andhra Pradesh, India

^b Department of Humanities and Sciences, K.S.R.M College of Engineering, Kadapa 516003, Andhra Pradesh, India

^c Department of Mathematics, Koneru Lakshmaiah Education Foundation, Hyderabad 500075, Telangana, India

^d Institute of Mathematics, Henan Academy of Sciences, Zhengzhou 450046, China

^e Industrial Mathematics Laboratory, Baikal School of BRICS, Irkutsk National Research Technical University, Irkutsk 664074, Russia

^f Nuclear Engineering and Fluid Mechanics Department, University of the Basque Country UPV/EHU, Nieves Cano 12, 01006 Vitoria-Gasteiz, Spain

ARTICLE INFO

Keywords:

Buoyancy forces
Permeable surface
Engine oil
Soret number

ABSTRACT

This study investigates the heat and mass transmission behavior in an unsteady magnetohydrodynamic (MHD) movement of nanofluids over an inclined permeable surface, with applications in enhancing thermal management systems such as automotive cooling and industrial heat exchangers. The model specifically examines the consequence of thermal diffusion (Soret effect) and buoyant forces on Cu and TiO₂ nanoparticles dispersed in engine oil. The governing equations, comprising velocity, energy, and concentration equations, are recast into nonlinear ODEs manipulating similitude adaptations. These ODEs are then solved through a standard perturbation method under appropriate boundary conditions. The key findings indicate that enhancing thermal radiation diminishes the velocity and temperature profiles, while raising chemical reaction rates decrease concentration levels. Additionally, higher Soret parameter values are associated with increased velocity and concentration. Quantitatively, TiO₂-engine oil nanofluids exhibit a 15% higher velocity compared to Cu-engine oil nanofluids, highlighting the superior performance of TiO₂ in dynamic thermal systems. Furthermore, numerical outcomes for the local skin contention, Nusselt numeral, and Sherwood digit are tabulated to illustrate the consequence of material properties. The outcomes of this study are particularly beneficial in optimizing the design of heat exchangers, improving fuel efficiency in automotive engines, and enhancing industrial processes where precise thermal control is critical.

1. Introduction

In engineering domains such as automotive chilling, industrial heat exchangers, and electronic device thermal management, efficient heat transfer is paramount for optimizing implementation and reducing energy consumption. Nanofluids, particularly those containing Cu and TiO₂ nanoparticles dispersed in engine oil, have shown promise in enhancing thermal conductivity and improving heat transfer rates. This study's mathematical model, which examines the effects of thermal diffusion and buoyant forces in such nanofluids, directly contributes to the design and optimization of these critical systems. By providing a deeper understanding of how these nanofluids behave under various

conditions, the research offers valuable insights that can lead to more efficient and cost-effective thermal management solutions in real-world engineering applications. The idea of boosting the heat conduction abilities of liquids by introducing ultra-fine, nanometer-sized particles was firstly suggested by Masuda et al. (Masuda et al., 1993) in 1993, later enhanced by Choi (Choi and Eastman, 1995) in 1995. This groundbreaking strategy gave rise to nanofluids, where the addition of nanoparticle dispersions into base fluids leads to a notable improvement in thermal conductivity. As highlighted by Eastman et al. (Eastman et al., 2001), these nanoparticle-infused liquids demonstrate an exceptional increase in thermal conductivity, nearly 40 % greater, in comparison to traditional fluids lacking such nanoparticles. This advancement has paved the way for the utilization of nanofluids in

* Corresponding authors.

E-mail addresses: kraghunath25@gmail.com (R. Kodi), vrcreddymaths77@gmail.com (R.R. Vaddemani), mathematicshari@gmail.com (H. Kommaddi), snoei@istu.edu (S. Noeiaghdam), unai.fernandez@ehu.es (U. Fernandez-Gamiz).

<https://doi.org/10.1016/j.jksus.2024.103434>

Received 26 June 2024; Received in revised form 3 September 2024; Accepted 4 September 2024

Available online 12 September 2024

1018-3647/© 2024 The Authors. Published by Elsevier B.V. on behalf of King Saud University. This is an open access article under the CC BY-NC-ND license (<http://creativecommons.org/licenses/by-nc-nd/4.0/>).

Nomenclature			
x, y	cartesian coordinates (m)	Pr	Prandtl factor
u^*, v^*	velocity components along x, y directions (m/s)	u	non-dimensional velocity
λ	the Casson fluid	v_0	suction velocity (m/s)
α	Angle of inclination	<i>Greek symbols</i>	
γ	aligned magnetic field	ρ	fluid density (Kg/m ³)
C^*	species concentration	β_T	coefficient of volume expansion
C_∞^*	fluid concentration far away from the wall	β_e	coefficient of volume expansion with concentration
C_w^*	fluid concentration of the wall	τ	Non-dimensional skin friction
C_p	specific heat at a constant pressure (J/kg. K)	θ	Non-dimensional temperature (K)
g	acceleration due to gravity (m/s ²)	$(\rho C_p)_{nf}$	heat capacitance of the nanofluid
K^*	permeability of a porous medium (m ²)	β_f and β_c	thermal expansion of the fluid and of the solid, respectively
T^*	temperature of the liquid (K)	ρ_f and ρ_c	densities of the fluid and of the solid fractions, respectively
Q	heat absorption (J/K)	μ_{nf}	viscosity of nanofluid
T_∞^*	fluid temperature far away from the wall	α_{nf}	thermal diffusivity of the nanofluid
Gm	mass Grashof factor	K_{nf}	thermal conductivity of the base fluid
Gr	thermal Grashof factor	β_{nf}	coefficient of thermal expansion of nanofluid
K_1	non dimensional rate of chemical reaction	K	thermal conductivity (W/m.K)
K_r	chemical reaction (W/mk)	ν	kinematic viscosity (m ² /s)
Sc	Schmidt factor	σ	electrical conductivity (S/m)
Sr	Soret number	μ	dynamic viscosity (Pa.s)
S	suction factor	<i>Subscripts and super scripts</i>	
B_0	magnetic field (A.m ²)	W	wall
M	magnetic field	∞	for away from the wall
R	radiation factor (cm ⁻²)	Prime	denotes differentiation with respect to
Nu	Nusselt factor		

diverse sectors that demand superior heat transfer capabilities.

In 2006, Buongiorno (Buongiorno, 2006) carried out an in-depth examination of the augmented thermal conductivity observed in nanofluids, attributing this improvement to the underlying mechanisms of Brownian movement and thermophoresis. He also familiarized a sophisticated model for the preservation of thermal emission, and tiny-particle concentration during the flow of nanofluids. Since this pivotal research, nanofluids have been increasingly utilized across a diverse array of industrial and medical disciplines, encompassing areas like microelectronics, fuel cell technology, pharmaceutical manufacturing, and state-of-the-art refrigerating strategies (Kumar and Kumar, 2018; Usman et al., 2018; Haile and Awgichew, 2019; Khan et al., 2019). Shekar et al. (Sudhanshu et al., 2022) newly delved into the complex Darcy–Forchheimer flow dynamics of radiative nanofluids optimized for minimal entropy production, taking into account secondary slip conditions, internal heat generation/absorption, and the influence of geometric parameters. Furthermore, Shaw et al. (Shaw et al., 2022) conducted a thorough investigation into the magnetohydrodynamic (MHD) flow behavior and thermal properties of hybrid nanofluids, examining various thermal radiation scenarios across a spectrum of Prandtl numbers. In a related study, Shaw and collaborators (Shaw et al., 2021) explored the computational effects of micro-rotation within Casson-Carreau nanofluids under MHD flow, including the impact of slip conditions on fluid behavior. Sastry and colleagues (Sastry et al., 2022) conducted research into the dynamic three-dimensional movement of micropolar nanofluids via a tightened track, an area of study with significant relevance to cardiovascular health applications. Similarly, Nayak et al. (Nayak et al., 2022) researched the consequences of slip momentum, thermo-radiative, MHD conditions on fluid dynamics about the stagnation significance movement along a stretching consistency, providing practical discernment into the demeanor of these advanced fluid systems in specialized engineering contexts.

The essence of thermo-transmission in nanofluids widely depends on the thermophysical possessions of the tiny-particles hovering in the underneath fluid, their interchanges within the host liquid, and the flow

characteristics of the resulting fluids. Zhang et al. (Zhang et al., 2024) studied 3D-MHD hybrid convection in a darcy-Horkheimer Maxwell liquid: thermophysical aspects and activation exuberance consequence. Raghunath et al. (Kodi et al., 2023) and Hari Babu et al. (Kommaddi et al., 2023) have enclosed thermal and material transmission on the MHD movement of Jeffrey nano-liquid founded on Cu and TiO₂ beyond a glad dish with thermo physical and radiation aspects. Additionally, studies on nanoparticle composition and rheology can be found in references (Balasundaram et al., 2023; Mohana Ramana et al., 2024; Francis et al., 2024; Dharmiaiah et al., 2023).

The determinations of this introspection hold momentous essences for various engineering applications, particularly in the development and optimization of thermal management systems where enhanced thermal conductivity and precise control of fluid dynamics are crucial. By analyzing the behavior of Cu-engine oil and TiO₂-engine oil nanofluids under the influence of thermal diffusion, buoyancy forces, and magnetohydrodynamic (MHD) effects, this research provides valuable insights that can be directly spread to enhance the efficiency of automotive chilling systems. In these systems, maintaining optimal engine temperatures is essential for enhancing fuel efficiency and reducing emissions, and the superior thermal conductivity of nanofluids like TiO₂-engine oil can recreate a dramatic position in achieving these goals. Moreover, the ability to control fluid flow with magnetic fields through MHD effects offers additional avenues for optimizing cooling processes, ensuring that heat is effectively dissipated even under challenging operating conditions. Ali et al. (Ali et al., 2018) introduced a fluid model based on the Brinkman equation to study the rheological impacts of nanofluids. They specifically examined the use of MoS₂ nanoparticles in motor oil and kerosene on a spinning surface. Vashghani et al. (Vashghani et al., 2013) used the hot wire technique to ascertain the density and heat transmission rates of TiO₂-engine oil nanofluids. They then corroborated their findings using experimental data. Khat et al. (Khata et al., 2020) conducted a recent inspection of the thermal behaviour capabilities of nanofluids made from water and motor oil. They examined different shapes and sizes of heat exchangers

with grooved surfaces, and tested them with varying flow rates of water and engine oil. Rajo et al. (Raju et al., 2020) conducted a comprehensive study on the thermal characteristics of engine oil (EO) nanoparticles. They examined the magnetic influences in a porosity channel. Ravi et al. (Ravindranath Reddy and Ramakrishna Reddy, 2022) investigated the characteristics of Casson tiny liquids in magnetohydrodynamic convection flow over a partially limitless slanted permeability movable plate, taking into account heat and energy transmission. Ahmad et al. (Ahmad et al., 2021) possessed the developments of copper (Cu) and titanium dioxide (TiO₂) in the flow of engine oil under thermal jump circumstances. Also many other related studies can be found in (Mansourian et al., 2022; Hoseininejad et al., 2021; Behrouz et al., 2023; Berrehal et al., 2024). Ramasekhar et al. (Ramasekhar et al., 2024) recently conducted a study on the heat transmission improvement of engine oil various nanoparticles placed in a permeable stretched cylinder. Ebrahim et al. (Algehyne et al., 2024) conducted an analysis on the quantitative exploration of gyrotactic microbes and the consequences of varying viscosity on the movement of chemically reacting nanoliquid. Ramasekhar et al. (Ramasekhar et al., 2024) have researched Numerical analysis of Casson liquid movement performance of blood containing gold and Fe₃O₄ nanofluid injected into a stenotic artery. In their study, Jawad et al. (Jawad et al., 2024) conducted a comprehensive analysis of the numerical simulation of Buongiorno's concept on Maxwell tiny fluids. The study focused on analysing heat and mass transport using Arrhenius power.

Thermal radiation and thermal diffusion are key mechanisms in heat transfer that have significant developments across miscellaneous enterprises. Thermal radiation involves the emission of heat in the form of electromagnetic waves, crucial in high-temperature processes like those found in energy production, combustion, and furnace operations. Thermo-diffusion, also comprehended as the Soret consequence, characterises the motion of particles within a liquid due to an energy gradient, affecting material composition and behavior. This phenomenon is essential in applications such as material processing, chemical engineering, and environmental control, where precise thermal management is required. Together, these processes play a vital role in optimizing heat transfer and improving the efficiency of technologies ranging from industrial heat exchangers to advanced thermal materials (Waseem et al., 2024; Ramasekhar et al., 2024).

Despite the foundational work by Ravindra and Ramakrishna (Ravindranath Reddy and Ramakrishna Reddy, 2022) on complimentary convection thermal and material transmission along inclined plates, there remains a significant gap in understanding how thermal diffusion and thermophysical properties influence this process under more complex and realistic conditions. Their study did not fully address the combined effects of these factors, particularly in scenarios involving porous media, radiation, and invariant heat generation under unsteady boundary conditions. Moreover, the behaviour of specific nanofluids, such as Cu-engine oil and TiO₂-engine oil, has not been thoroughly analyzed in this context. This gap is critical because these conditions are commonly encountered in practical engineering applications, where accurate predictions of heat and mass transfer are essential for optimizing system performance. By extending their investigation to include these variables and employing analytical methods to solve the governing equations, this study aims to furnish deeper discernment into the flow dynamics and enhance the understanding of how these parameters impact velocity, thermal and material transmission in nanofluid systems.

2. Mathematical Formulation

The study believes the inconsistent MHD two-dimensional movement of a streamlined, dense, incompressible, electronically manipulating liquid over a semi-unbounded abrupt penetrable surface embedded in a stationary permeable medium is considered under the influence of a constant rotating magnetic field, thermal aspects, and a

chemical reaction. The axis of y^* is perpendicular to the ascending tendency of the fluid. A uniform external capacitive field B_0 is applied with the y -direction, with a mealy induced capacitive field and external electronic field due to charge separation power.

- This revision enhances the overall readability and clarity while preserving the technical integrity of the original text. Please let me know if any further adjustments are needed.
- In this scenario, the magnetic flux is applied in a lateral orientation, and the capacitive Reynolds constant is presumed to be extremely tiny. As a result, the effects of magnetic diffusion and the Hall consequence are considered negligible.
- The nanoliquid composed of motor oil as the base, incorporating copper (Cu) and titanium oxide (TiO₂) nanostructures.
- With the exception of the change in density that occurs with temperature, it is expected that the characteristics of the fluid would stay unchanged.
- Given that the concentration of the dispersing substance is tiniest resembled to different chemical components, the thermal diffusion and diffusion-thermo effects are disregarded. Additionally, the concentration in the region distant from the wall (C_∞) is found to be exceptionally low.
- As a result of the presumption of a semi-infinite plane, the flow characteristics are only dependent on y^* and time t^* .
- With the use of the Boussinesq approximation, which was developed by Ravindra and Ramakrishna (Ravindranath Reddy and Ramakrishna Reddy, 2022), a chemical reaction takes place inside the flow. In this equation, all thermo-physical characteristics are regarded constant with respect to the linear momentum equation.

By using the Boussinesq approximation, which was used by Ravindra and Ramakrishna (Ravindranath Reddy and Ramakrishna Reddy, 2022), a chemical reaction takes place inside the flow. In this particular paradigm, it is understood that all thermophysical parameters are believed to be consistent relative to the linear momentum model.

$$\frac{\partial v^*}{\partial y^*} = 0 \quad (1)$$

$$\frac{\partial u^*}{\partial t^*} + v^* \frac{\partial u^*}{\partial y^*} = -\frac{\mu_{nf}}{\rho_{nf}} \left(1 + \frac{1}{\lambda} \right) \frac{\partial^2 u^*}{\partial y^{*2}} + \frac{1}{\rho_{nf}} \left(\frac{g\beta_T}{(g\beta_C)_{nf}} (T^* - T_\infty^*) + \frac{1}{(g\beta_C)_{nf}} (C^* - C_\infty^*) \right) \text{Cos}\alpha - \frac{\sigma B_0^2}{\rho_{nf}} \text{Sin}^2 \gamma u^* - \frac{\mu_{nf}}{\rho_{nf}} \frac{u^*}{k^*} \quad (2)$$

$$\left(\frac{\partial T^*}{\partial t^*} + v^* \frac{\partial T^*}{\partial y^*} \right) = \alpha_{nf} \frac{K}{(\rho C_p)_{nf}} \frac{\partial^2 T^*}{\partial y^{*2}} - \frac{1}{(\rho C_p)_{nf}} \frac{\partial q_r^*}{\partial y^*} + \frac{Q^*}{(\rho C_p)_{nf}} (T^* - T_\infty^*) \quad (3)$$

$$\frac{\partial C^*}{\partial t^*} + v^* \frac{\partial C^*}{\partial y^*} = D \frac{\partial^2 C^*}{\partial y^{*2}} - K^* (C^* - C_\infty^*) + D_1 \frac{\partial^2 T^*}{\partial y^{*2}} \quad (4)$$

When the prior presumptions are taken into consideration, the following are the matching limit specifications for the spatial distribution of speed, energy, and specialisation:

$$t^* < 0, C^* = C_\infty^*, u^*(y^*, t^*) = 0, T^* = T_\infty^*$$

$$t^* \geq 0, C^* = C_w^* + \varepsilon (C_w^* - C_\infty^*) e^{m^* t^*}, T^* = T_w^* + \varepsilon (T_w^* - T_\infty^*) e^{m^* t^*}, u^*(y^*, t^*) = u_0 \text{ at } y^* = 0 \quad (5)$$

$$T^* \rightarrow T_\infty^*, u^*(y^*, t^*) = 0, C^* \rightarrow C_\infty^* \text{ as } y^* \rightarrow \infty \quad (6)$$

Table 1

Thermo-material possessions (see (Abbasi et al., 2015; Abbasi et al., 2015; Ahmad et al., 2021).

Materials	ρ (kg/m ³)	C_p (J/kgK)	k (W/mK)
Engine oil (EO)	884	385.00	401.00
Copper (Cu)	8933	1910.1	0.1441
Titanium oxide (Ti O2)	4250.5	686.200	8.9539

Table 2

It is necessary to propose connections between engine oil nanoparticles based on copper and titanium dioxide (Abbasi et al., 2015; Abbasi et al., 2015; Ahmad et al., 2021).

Properties	Nanofluid specifications
Density	$\rho_{nf} = (\rho_f - \rho_f\varphi) + \varphi\rho_s$,
Heat capacity	$(\rho C_p)_{nf} = (\rho C_p)_f(1 - \varphi) + (\rho C_p)_s\varphi$,
Thermo heat capacity	$(\rho\beta)_{nf} = (\rho\beta)_f(1 - \varphi) + (\rho\beta)_s\varphi$
Thermal conductivity	$K_{nf} = K_f \left(\frac{K_s + 2K_f - 2\varphi(K_f - K_s)}{K_s + 2K_f + 2\varphi(K_f - K_s)} \right)$,
Absolute viscosity	$\mu_{nf} = \left(\frac{\mu_f}{(1 - \varphi)^{2.5}} \right)$,
Electrical conductivity	$\alpha_{nf} = \left(\frac{K_{nf}}{(\rho C_p)_{nf}} \right)$

For the purpose of code validation, the thermophysical characteristics of engine oil, copper, and titanium are shown in Table 1. According to Abbasi (Abbasi et al., 2015);(Abbasi et al., 2015) , and Ahamed et al. (Ahmad et al., 2021), these factors are explicitly described in a precise manner. Table 2. Table 3.

Frequently – v_0 is applied in this scenario to represent the standard speed at the surface. This speed is favorable when suction is present (v_0 is greater than 0), but it is unfavorable when botching infusion is present (v_0 is less than 0).

The mathematical model that Cramer and Pai (Cramer and Pai, 1973) devised for an optically flimsy dismal gas that is near to counterbalance is the subject of our investigation. The authors Grief et al. (Grief et al., 1971) went into additional detail about this paradigm.

$$\frac{\partial q_r^*}{\partial y^*} = 4(T^* - T_w^*) I \tag{7}$$

It is necessary to add the dimensionless values that result from the physical situation in order to standardise the mathematical illustration of the scenario.

$$u = \frac{u^*}{U_0}, v = \frac{v^*}{\nu_0}, y = \frac{\nu_0 y^*}{v_f}, t = \frac{t^* \nu_0^2}{v_f}, \theta = \frac{T^* - T_\infty^*}{T_w^* - T_\infty^*} \varphi = \frac{C^* - C_\infty^*}{C_w^* - C_\infty^*}, n = \frac{n^* \vartheta_f}{\nu_0^2}, S = \frac{\nu_0}{U_0} \tag{8}$$

$$k = \frac{k^* \nu_0^2}{v_f^2}, Pr = \frac{\mu_f C_{pf}}{K_f}, Sc = \frac{v_f}{D_m}, M = \frac{\sigma B_0^2 v_f}{\rho_f \nu_0^2}, Q = \frac{Q^* v_f}{(\rho C_p)_f \nu_0^2}, Kr = \frac{v_f K^*}{\nu_0^2}, Rd = \frac{4I_1 v_f}{(\rho C_p)_f \nu_0^2}, Sr = \frac{D_1 K(T_w^* - T_\infty^*)}{v_f (C_w^* - C_\infty^*)}, Gr = \frac{v_f g(\rho\beta_T)_f (T_w^* - T_\infty^*)}{U_0 \nu_0^2}, Gm = \frac{v_f g(\rho\beta_c)_f (C_w^* - C_\infty^*)}{U_0 \nu_0^2} \tag{8}$$

Table 3

The significance of numerous abundances of skin conflict.

Gr	M	K	Sr	Rd	Kr	Gm	Q	Skin Friction for copper water liquid current outcomes	Skin Friction for Titanium oxide liquid current outcomes	Skin Friction for copper-Engine oil Ravindra and Ramakrishna (Ravindranath Reddy and Ramakrishna Reddy, 2022) values	Skin Friction for Titanium oxide-Engine oil Ravindra and Ramakrishna (Ravindranath Reddy and Ramakrishna Reddy, 2022) values
3	0.5	2	1.5	1	0.5	3	0.5	0.1175	0.3012	0.1175	0.3012
6	0.5	2	1.5	1	0.5	3	0.5	1.9225	1.5165	1.9225	1.5165
9	0.5	2	1.5	1	0.5	3	0.5	3.9568	3.3045	3.9568	3.3045
5	1	2	1.5	1	0.5	3	0.5	4.2675	4.2387	4.2675	4.2387
5	2	2	1.5	1	0.5	3	0.5	1.9475	1.5197	1.9475	1.5197
5	3	2	1.5	1	0.5	3	0.5	0.4625	0.0446	0.4625	0.0446
5	0.5	3	1.5	1	0.5	3	0.5	1.9212	1.5151	1.9212	1.5151
5	0.5	4	1.5	1	0.5	3	0.5	3.0112	2.6845	3.0112	2.6845
5	0.5	6	1.5	1	0.5	3	0.5	3.5752	3.3652	3.5752	3.3652
5	0.5	2	1	1	0.5	3	0.5	0.7550	0.4525	0.7550	0.4525
5	0.5	2	3	1	0.5	3	0.5	5.4653	4.6878	5.4653	4.6878
5	0.5	2	5	1	0.5	3	0.5	10.2652	8.9598	10.2652	8.9598
5	0.5	2	1.5	1	0.5	3	0.5	1.4775	1.1885	1.4775	1.1885
5	0.5	2	15	0.2	0.5	3	0.5	1.5852	1.2446	1.5852	1.2446
5	0.5	2	1.5	0.3	0.5	3	0.5	1.7152	1.3152	1.7152	1.3152
5	0.5	2	1.5	1	1	3	0.5	0.0361	0.2445	0.0361	0.2445
5	0.5	2	1.5	1	5	3	0.5	2.0575	2.1352	2.0575	2.1352
5	0.5	2	1.5	1	10	3	0.5	2.2295	2.2678	2.2295	2.2678
5	0.5	2	1.5	1	0.5	2	0.5	0.9856	0.9882	0.9856	0.9882
5	0.5	2	1.5	1	0.5	4	0.5	1.9352	1.4124	1.9352	1.4124
5	0.5	2	1.5	1	0.5	6	0.5	2.8245	2.1845	2.8245	2.1845

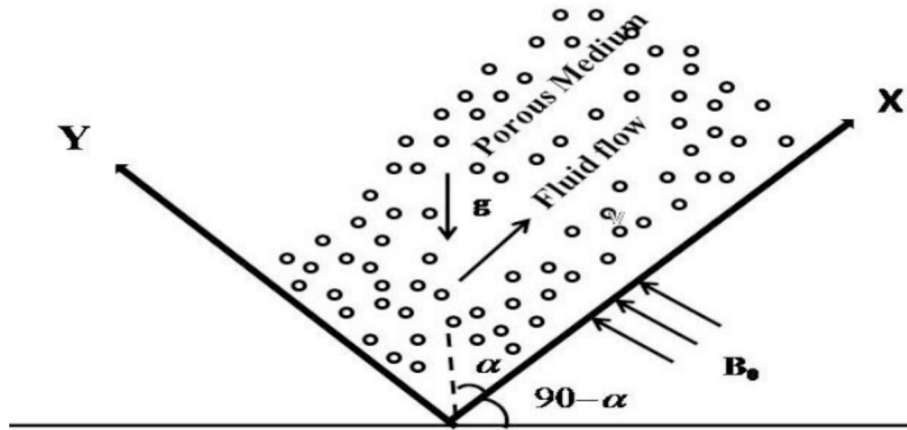


Fig. 1. Depicts the physical structure of the phenomena.

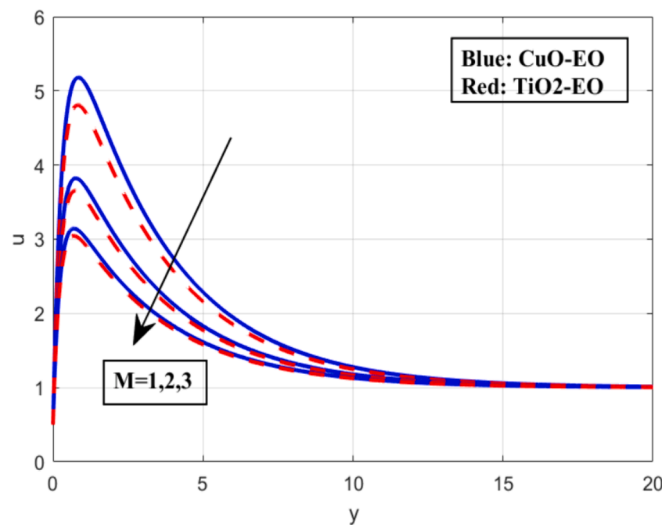


Fig. 2a. Flow velocity contours for magnetic strength.

In their original, non-dimensional form, the characteristics (2) to (4) are as follows:

$$A \left(\frac{\partial u}{\partial t} - S \frac{\partial u}{\partial y} \right) = D \left(1 + \frac{1}{\lambda} \right) \frac{\partial^2 u}{\partial y^2} + B (Gr\theta + Gm\varphi) \cos\alpha + u (M \sin^2 \gamma + 1/k) \tag{9}$$

$$C \left(\frac{\partial \theta}{\partial t} - S \frac{\partial \theta}{\partial y} \right) = \frac{1}{Pr} \left(E \frac{\partial^2 \theta}{\partial y^2} - (R_d + Q) \theta \right) \tag{10}$$

$$\frac{\partial \varphi}{\partial t} - S \frac{\partial \varphi}{\partial y} = \frac{1}{Sc} \frac{\partial^2 \varphi}{\partial y^2} + Sr \frac{\partial^2 \varphi}{\partial y^2} - Kr\varphi \tag{11}$$

$$A = \left((1 - \varphi) + \varphi \left(\frac{\rho_s}{\rho_f} \right) \right) B = \left((1 - \varphi) + \varphi \left(\frac{(\rho\beta)_s}{(\rho\beta)_f} \right) \right) C = \left((1 - \varphi) + \varphi \left(\frac{(\rho C_p)_s}{(\rho C_p)_f} \right) \right)$$

$$D = \left(\frac{1}{(1 - \varphi)^{2.5}} \right), D = \left(\frac{1}{(1 - \varphi)^{2.5}} \right)$$

The boundary circumstances that are associated with this are specified

as follows:

$$t^* < 0, \theta = 0, u = 0, \varphi = 0$$

$$t^* \geq 0, u = 1, \theta = 1 + \varepsilon e^{\text{int}}, \varphi = 1 + \varepsilon e^{\text{int}} \text{ at } y = 0 \tag{12}$$

$$u = 0, \theta \rightarrow 0, \varphi \rightarrow 0 \text{ as } y \rightarrow \infty \tag{13}$$

3. Method of solution

Equations (10) through (12) are PDE's that cannot be directly resolved with a closed-form expression. These equations can be addressed by transforming them into a sequence of ODEs utilizing the perturbation technique. This strategy allows for the breakdown of complex problems into simpler ones by introducing small perturbations to the system, enabling an approximate solution.

$$\begin{aligned} u(y, t) &= u_0(y) + \varepsilon u_1(y) e^{\text{int}} + O(\varepsilon^2) \\ \theta(y, t) &= \theta_0(y) + \varepsilon \theta_1(y) e^{\text{int}} + O(\varepsilon^2) \\ \varphi(y, t) &= \varphi_0(y) + \varepsilon \varphi_1(y) e^{\text{int}} + O(\varepsilon^2) \end{aligned} \tag{14}$$

As a result of this transformation, the distributions of momentum, thermal energy, and solute concentration within the system can be articulated through a combination of harmonic and non-harmonic processes. These processes capture both the regular oscillatory behaviors and more complex, irregular dynamics within the system, providing a comprehensive understanding of the underlying physical phenomena.

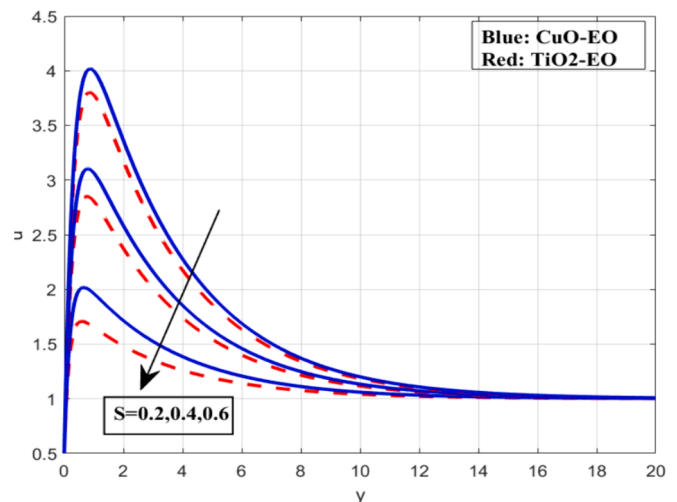


Fig. 2b. Flow velocity contours for Suction factor.

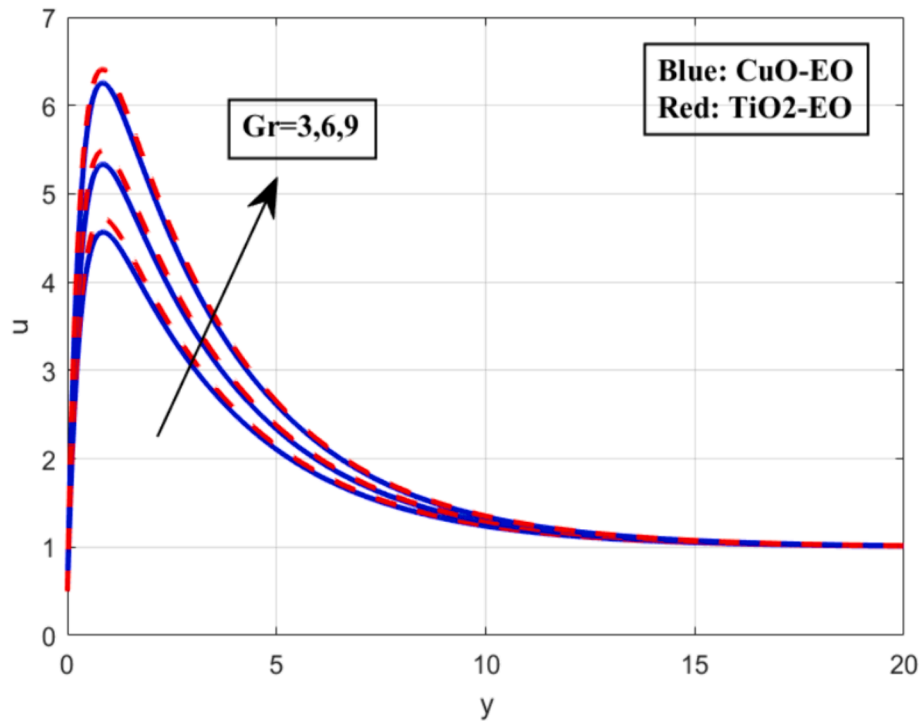


Fig. 3a. Flow velocity contours for Thermal Grashof Numeral.

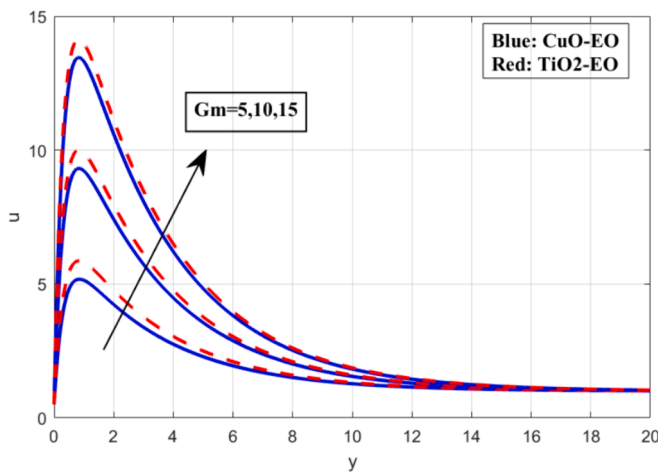


Fig. 3b. Flow velocity contours for Mass Grashof Numeral.

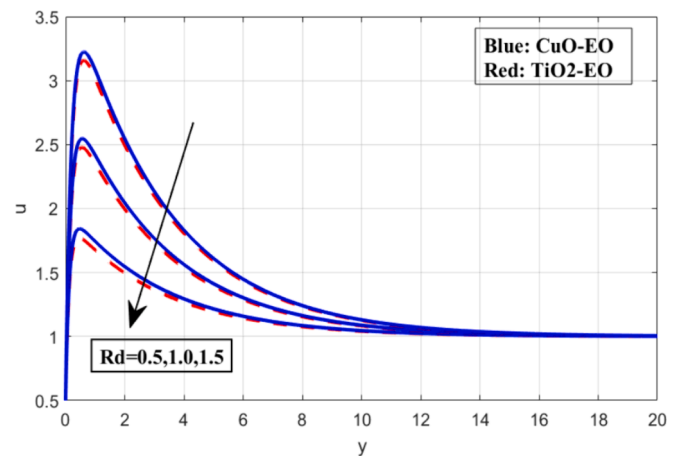


Fig. 4a. Flow velocity contours for thermal radiation.

This approach facilitates the analysis of the system's behavior under varying conditions, offering insights that would be difficult to obtain through direct analytical solutions.

$$D \left(1 + \frac{1}{\lambda} \right) u_0'' + A S u_0' - \left(M + \frac{1}{k} \right) u_0 = -B(Gr \cos \alpha \theta_0 + Gm \cos \alpha \varphi_0) - \left(M \sin^2 \gamma + \frac{1}{k} \right) \quad (15)$$

$$E \theta_0'' + Pr C S \theta_0 - Pr(R_d + Q) \theta_0 = 0 \quad (16)$$

$$\phi_0'' + SS_c \phi_0' - Sc Kr \phi_0 = -Sc Sr \theta_0'' \quad (17)$$

$$D \left(1 + \frac{1}{\lambda} \right) u_1'' + A S u_1' - \left((M + 1/k) u_1 + A n u_1 \right) = -B(Gr \theta_1 + Gm \varphi_1) \cos \alpha - u_0' - \left(M \sin^2 \gamma + \frac{1}{k} \right) \quad (18)$$

$$\frac{1}{Pr} E \theta_1'' + S C \theta_1' - (n \theta_1 + Q \theta_1) + \theta_0' = 0 \quad (19)$$

$$\phi_1'' + S S_c \phi_1' - Sc (Kr + n) \phi_1 = -Sc \phi_0' - Sc Sr \theta_1'' \quad (20)$$

The boundary constraints that are linked with it are

$$u_0 = 1, u_1 = 1, \theta_0 = 1, u_1 = 0, \varphi_1 = 1, \theta_1 = 1, \text{ at } y = 0 \quad (21)$$

$$u_0 \rightarrow 0, \theta_0 \rightarrow 0, u_1 \rightarrow 0, \varphi_1 \rightarrow 0, \theta_1 \rightarrow 0, \varphi_0 \rightarrow 0 \text{ as } y \rightarrow \infty \quad (22)$$

We are able to determine the momentum, energy, and concentration

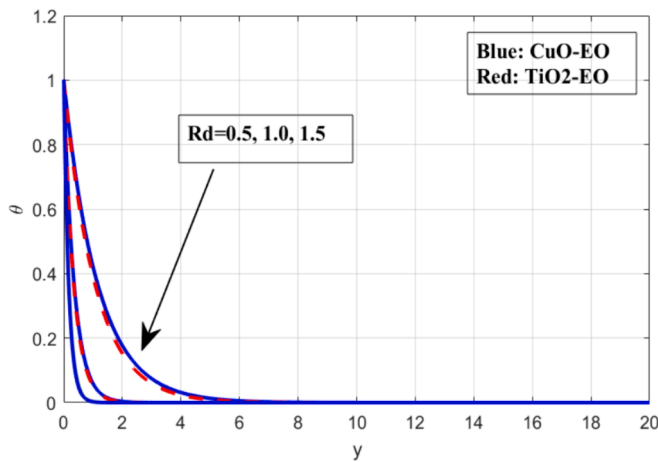


Fig. 4b. Flow temperature contours for thermal radiation.

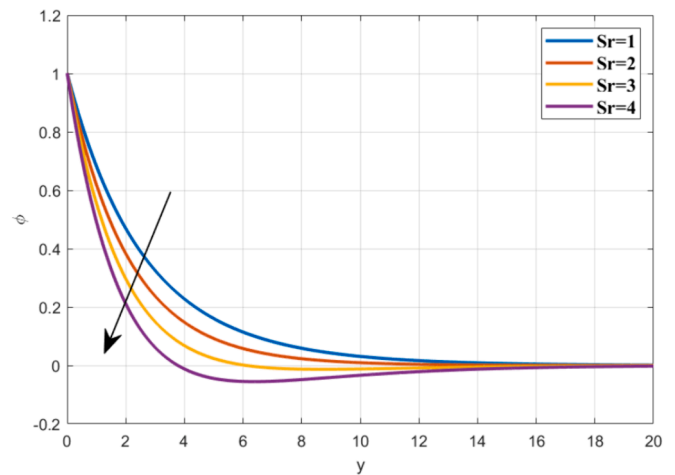


Fig. 5b. Flow concentration contours for solet numeral.

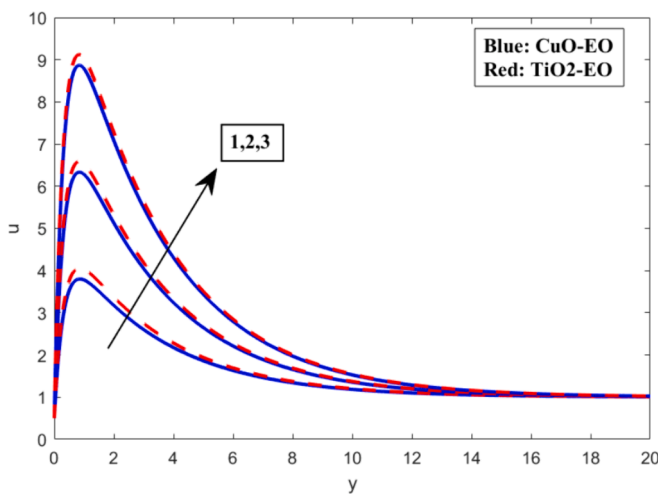


Fig. 5a. Flow velocity contours for solet numeral.

that are contained inside the boundary layer by resolving characteristics (15–20) using the boundary circumstances (21–22).

$$u = 1 + b_{11}\exp(-m_5y) + b_9\exp(-m_1y) + b_{10}\exp(-m_3y) + \epsilon e^{\text{int}} \left[\begin{array}{l} (1 + b_{14}\exp(-m_3y) + b_{17}\exp(-m_6y) + \\ b_{12}\exp(-m_1y) + b_{13}\exp(-m_2y) + \\ b_{15}\exp(-m_4y) + b_{16}\exp(-m_5y) \end{array} \right] \quad (23)$$

$$\theta = b_4\exp(-m_3y) + b_3\exp(-m_1y) + \epsilon e^{\text{int}} \left[\begin{array}{l} b_6\exp(-m_2y) + b_8\exp(-m_4y) + \\ b_5\exp(-m_1y) + b_7\exp(-m_3y) \end{array} \right] \quad (24)$$

$$\varphi = \exp(-m_1y) + [\epsilon e^{\text{int}} b_2\exp(-m_2y) + \epsilon e^{\text{int}} b_1\exp(-m_1y)] \quad (25)$$

Significant physical elements involved at the border boundary include the skin frictional and the Nusselt value, often described in a non-dimensional arrangement. Skin friction generates both of these parameters. Fig. 1

$$\tau = \left(\frac{\partial u}{\partial y} \right)_{y=0} = (-m_1b_9 - m_3b_{10} - m_5b_{11}) - \left(\epsilon e^{\text{nt}} m_1 b_{12} + \epsilon e^{\text{nt}} m_2 b_{13} + \epsilon e^{\text{nt}} m_3 b_{14} + \epsilon e^{\text{nt}} m_4 b_{15} + \epsilon e^{\text{nt}} m_5 b_{16} + \epsilon e^{\text{nt}} m_6 b_{17} \right) \quad (32)$$

$$Nu = - \left(\frac{\partial \theta}{\partial y} \right)_{y=0} = m_1b_3 + m_3b_4 + \epsilon e^{\text{int}} (m_1b_5 + m_2b_6 + m_3b_7 + m_4b_8) \quad (33)$$

4. Results and discussion

To obtain profound insights into the concern, we executed numerical mensuration for the dimensionless momentum, thermal profile, and species concentration, along with the skin conflict coefficient and Nusselt numeral, applying precise parameter configurations for two distinct nanofluids based on engine oil. We developed solutions for both TiO2-engine oil and Cu-engine oil nanoliquids, as demonstrated in Figs. 2-6. The thermo-material characteristics of the engine oil and the tiny-particles (Cu and TiO2) are presented in Table 1. To substantiate our findings, we cross-referenced the skin conflict characteristic and local Nusselt numeral with the results obtained by Ravi and krishna (Ali et al., 2018) under numerous scenarios, as expressed in Table 4. This variation indicates an excellent correlation, thereby affirming the accuracy and robustness of our analysis.

Fig. 2a presents the velocity profiles of nanofluids comprising Cu-engine oil and TiO2-engine oil nanoparticles under varying magnetic field strengths (M). The results indicate a clear reduction in nanofluid velocity as the magnetic field intensity increases, a phenomenon attributed to the Lorentz force generated in the electrically conductive nanofluids underneath the consequence of the capacitive field. This strength operates opposite to the liquid's motion, creating a drag effect that slows down the flow. The extent of this velocity reduction reflects the increased resistance imposed by the capacitive field, which is more pronounced as the capacitive intensity rises. Both Cu and TiO2 nanoparticles exhibit this behavior, though the specific response may differ due to their distinct electrical and thermal properties. These findings have significant implications for applications in thermal management, such as in automotive cooling systems and industrial heat exchangers, where magnetic field adjustments could be employed to modulate fluid velocity and optimize heat transfer processes. This highlights the

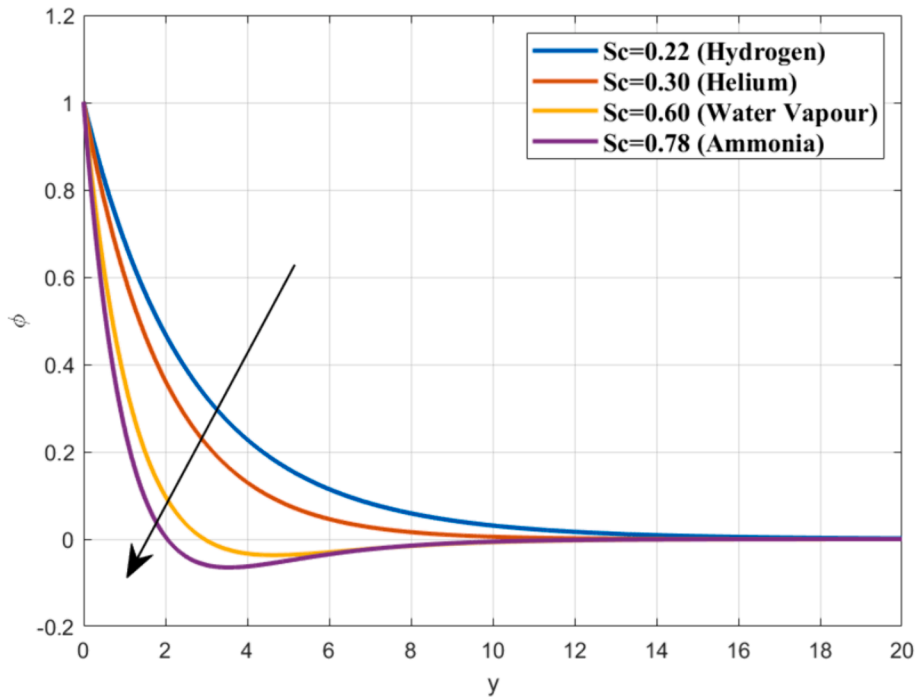


Fig. 6a. Flow concentration contours for Schmidt numeral.

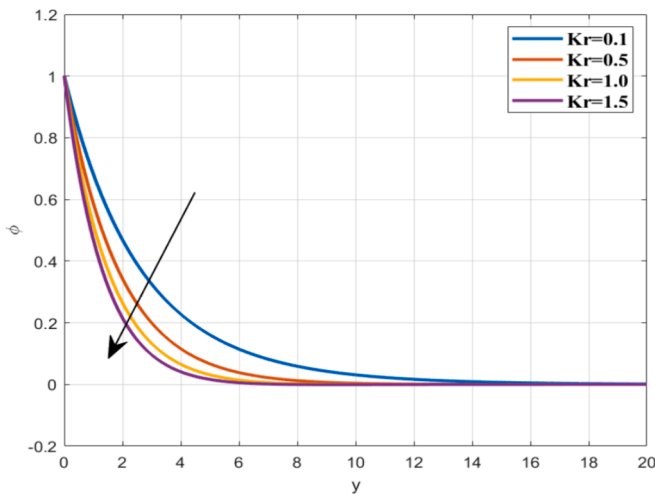


Fig. 6b. Flow concentration contours for Chemical reaction.

importance of considering magnetic effects when designing nanofluid-based systems for precise thermal control.

Fig. 2b illustrates the consequence of the suction parameter (S) on the fluid momentum within the boundary layer. The outcomes reveal that an enlargement in the suction factor oversees to a reduction in fluid velocity across the perimeter layer. This effect is consistent for both the base fluid and nanofluids containing Cu-engine oil and TiO₂-engine oil nanoparticles. The decrease in velocity with higher suction can be particular to the intensified removal of fluid from the periphery layer, which effectively thins the coating and reduces the momentum of the fluid particles. This behavior is crucial in applications where controlling the boundary layer thickness and liquid momentum is essential for optimizing heat transfer and flow stability in systems utilizing nanofluids.

Figs. 3a and 3b depict the consequences of the thermal Grashof numeral (Gr) and the mass Grashof numeral (Gm) on the momentum

Table 4

The significance of numerous abundances on the nusselt numeral.

R _d	Q	Gr	Gm	Nusselt values for copper water liquid current phenomena	Nusselt values for Titanium oxide water liquid current phenomena
1.5	1.0	3	5	0.45232	0.55366
2.0	1.0	3	5	0.89854	0.61075
2.5	1.0	3	5	2.23457	1.78353
1.5	3	3	5	0.94926	1.46562
1.5	4	3	5	1.49053	1.94254
1.5	5	3	5	2.41246	2.37678
1.5	1.0	2.5	5	0.98838	0.99467
1.5	1.0	5.0	5	0.87279	0.84563
1.5	1.0	7.5	5	0.72353	0.74355
1.5	1.0	3	2.5	0.99945	0.94746
1.5	1.0	3	5.0	0.84066	0.84283
1.5	1.0	3	7.5	0.73287	0.81201

distribution of nanofluids containing Cu-engine oil and TiO₂-engine oil. The findings indicate that an enhances in both (Gr) and (Gm) values oversees to an enhancement in the fluid velocity. This behavior can be explained by the buoyancy forces that are directly proportional to the Grashof numbers. As (Gr) and (Gm) upsurge, the buoyant significances evolve stronger, driving the fluid motion more vigorously and thereby increasing the velocity. This effect is observed in both nanofluids, demonstrating that higher thermal and mass Grashof numbers significantly influence the velocity distribution, which is particularly relevant for applications involving natural convection where buoyancy-driven flows are critical.

Figs. 4a and 4b illustrate the consequences of thermo-radiative on the momentum and energy distribution in nanofluids containing Cu-engine oil and TiO₂-engine oil. The results show that as the thermal radiation factor enhances, both the momentum and temperature of the fluids decrease. This reduction occurs because higher thermal radiation leads to greater heat emission from the fluids, resulting in a drop in their temperature. Consequently, the decrease in temperature reduces the thermal buoyancy forces, which in turn lowers the fluid velocity. This

behavior is significant in applications where controlling the heat dissipation and flow characteristics of nanofluids is essential, as increased thermal radiation can effectively regulate the temperature and velocity within the system.

Figs. 5a and 5b depict the influence of thermal diffusion on the momentum and concentration profiles of nanofluids containing Cu-engine oil and TiO₂-engine oil. The results indicate that increasing the sores factor enhances to an enhancement in the momentum and concentration of the nanofluids. This occurs because the sores number, also known as the thermo-diffusion, drives mass transfer in response to temperature gradients. As the thermal diffusion parameter rises, the movement of nanoparticles within the fluid is accelerated, leading to an enlargement in both the liquid's momentum and the concentration of nanoparticles. This effect emphasizes the noteworthy position of thermal diffusion in enhancing the transport properties of nanofluids, which can be particularly beneficial in applications requiring efficient heat and mass transfer.

Fig. 6a presents the concentration boundary layer profiles for H₂, H₂O, and NH₃, depicting the spatial distribution of concentration within the flow field. The comparison of these curves reveals that an increase in the Schmidt number results in a reduction in the thickness of the concentration boundary layer across all cases. This thinning of the boundary layer occurs because a higher Schmidt number corresponds to a lower mass diffusivity relative to momentum diffusivity, leading to a sharper concentration gradient near the surface. Consequently, substances with higher Schmidt numbers exhibit a more confined and thinner concentration boundary layer, which has significant implications for processes involving mass transfer, where precise control of concentration profiles is required. Fig. 6b illustrates the concentration profiles for different values of the disruptive chemical reaction parameter (Kr). The results show that increasing the chemical reaction parameter leads to a decrease in the concentration of the fluid. This reduction occurs because a higher (Kr) enhances the rate of the chemical reaction, which in turn consumes more of the reactant species, thereby lowering their concentration within the fluid. This behavior is particularly important in chemical engineering applications where controlling the concentration of reactive species is critical for optimizing reaction rates and ensuring desired outcomes in the process.

5. Conclusion

To enhance the examination, we considered two distinct types of nanofluids: TiO₂-engine oil and Cu-engine oil. The key findings are as follows:

- The velocity of the fluid reduces as the magnetic field intensity and suction value increase for both copper and titanium dioxide nanoparticles.
- On the contrary, when the thermal Grashof quantity, mass Grashof quantity, and sores numeral are increased to greater values, the momentum of the fluid rises.
- When the thermal radiation factor is increased, it outcomes in a fall in both the momentum and energy inside the liquid. This highlights the fact that as the thermal radiation gets more evident, the liquid's motion slows down, and the total temperature lowers.
- A rising in the sores numeral directs to enhance in both the momentum and concentration levels beyond the liquid. This suggests that a greater thermal dispersion increases the motion of the fluid and rises the concentration levels.
- Increasing the Schmidt number and the pace of the chemical reaction leads to a fall in concentration, which implies that more elevated Schmidt numeral and more intensive chemical retorts direct to diminish concentration stations within the liquid.
- The skin friction factor is markedly affected by both thermal conductivity and magnetic flux, indicating that changes in the intensity

of the magnetic field and heat transfer significantly impact the skin friction factor within the flow.

6. Future scope and limitations of this study

- The future scope of this study includes exploring the application of different nanofluids, considering three-dimensional flows, variable magnetic fields, and non-Newtonian base fluids to enhance the understanding and applicability of the findings.
- Further research could investigate the interaction of multiple nanoparticles to achieve synergistic effects in thermal management systems, with potential applications in electric vehicles, aerospace, and energy-efficient industrial processes.
- However, the study is limited by its focus on laminar flow and specific nanofluids (Cu and TiO₂ in engine oil), which may not fully capture the complexities of turbulent flows or generalize to other combinations.
- The uniform magnetic field assumption and the neglect of nanoparticle size and shape variations also present limitations.
- Additionally, practical implementation may require further experimental validation and consideration of economic factors such as the cost and scalability of nanofluid production.

Funding

Samad Noeiaghdam was supported by the Ministry of Science and Higher Education of Russian Federation (Project No. FZZS-2024-0003). U.F.-G. was supported by the Mobility Lab Foundation, a governmental organization of the Provincial Council of Araba and the local council of Vitoria-Gasteiz.

CRediT authorship contribution statement

Raghunath Kodi: Writing – review & editing, Writing – original draft, Validation, Software, Methodology. **Ramachandra Reddy Vad-demani:** Writing – review & editing, Validation, Methodology, Formal analysis. **Haribabu Kommaddi:** Writing – review & editing, Validation, Software, Methodology. **Samad Noeiaghdam:** Writing – review & editing, Validation, Software, Methodology, Formal analysis. **Unai Fernandez-Gamiz:** Writing – review & editing, Validation, Methodology, Formal analysis.

Declaration of Competing Interest

The authors declare that they have no known competing financial interests or personal relationships that could have appeared to influence the work reported in this paper.

References

- Abbasi, F.M., Hayat, T., Alsaadi, F., 2015. Hydromagnetic peristaltic transport of water-based nanofluids with slip effects through an asymmetric channel. *Int. J. Mod. Phys. B* 29, 1–17.
- Abbasi, F.M., Hayat, T., Alsaadi, F., 2015. Peristaltic transport of magnetonanoparticles submerged in water: model for drug delivery system. *Physica E* 68, 123–132.
- Ahmad, S., Ali, K., Nisar, K.S., Faridi, A.A., Khan, N., Jamsheed, W., Yunus Khan, T.M., Saleel, C.A., 2021. Features of Cu and TiO₂ in the flow of engine oil subject to thermal jump conditions. *Sci. Rep.* 11, 19592. <https://doi.org/10.1038/s41598-021-99045-x>.
- Algehyne, E.A., Jawad, M., Mureed, M., Gull, H., Saeed, S., 2024. Computational exploration of gyrotactic microbes and variable viscosity effects on flow of chemically reactive nanofluid. *BioNanoSci.* <https://doi.org/10.1007/s12668-024-01520-y>.
- Ali, F., Aamina, I., Khan, N.A., Sheikh, M.G., Tlili, I., 2018. Effects of different shaped nanoparticles on the performance of engine-oil and kerosene-oil: a generalized brinkman-type fluid model with non-singular kernel. *Sci. Rep.* 8, 15285.
- Balasundaram, H., Sathyamoorthi, S., Fernandez-Gamiz, U., Noeiaghdam, S., Sundar Santra, S., 2023. Hydrocephalic cerebrospinal fluid flowing rotationally with pulsatile boundaries: a mathematical simulation of the thermodynamical approach. *Theor. Appl. Mech. Lett.* 13, 100418 <https://doi.org/10.1016/j.taml.2022.100418>.

- Behrouz, M., Dinarvand, S., Yazdi, M.E., Tamim, H., Pop, I., Chamkha, A.J., 2023. Mass-based hybridity model for thermomicro-polar binary nanofluid flow: first derivation of angular momentum equation. *Chin. J. Phys.* 83, 165–184.
- Berrehal, H., Karami, R., Dinarvand, S., Pop, I., Chamkha, A., 2024. Entropy generation analysis for convective flow of aqua Ag-CuO hybrid nanofluid adjacent to a warmed down-pointing rotating vertical cone. *Int. J. Numer. Methods Heat Fluid Flow* 34 (2), 878–900.
- Buongiorno, J., 2006. Convective transport in nanofluids. *ASME J. Heat Transf.* 128, 240–250.
- Choi, U.S., Eastman, J.A., 1995. Enhancing Thermal Conductivity of Fluids with Nanoparticles 95, 1135.
- Cramer, K.P., Pai, S.I., 1973. *Magneto Fluid Dynamics for Engineers and Applied Physics*. McGraw-Hill Book Co, New York.
- Dharmaiah, G., Prasad, J.R., Balamurugan, K.S., Nurhidayat, I., Fernandez-Gamiz, U., Noeiaghdam, S., 2023. Performance of magnetic dipole contribution on ferromagnetic non-Newtonian radiative MHD blood flow: an application of biotechnology and medical sciences. *Heliyon* 9, e13369.
- Eastman, J.A., Choi, U.S., Li, S., Yu, W., Thompson, L.G., 2001. Anomalously increased effective thermal conductivities of ethylene glycol-based nanofluids containing copper nanoparticles. *Appl. Phys. Lett* 78, 718–720.
- Francis, P., Sambath, P., Fernandez-Gamiz, U., Noeiaghdam, S., Dinarvand, S., 2024. Computational analysis of bio-convective Eyring-Powell nanofluid flow with magneto-hydrodynamic effects over an isothermal cone surface with convective boundary condition. *Heliyon* 10, e25088.
- Grief, G., Habib, I.S., Lin, L.C., 1971. Laminar convection of a radiating gas in a vertical channel. *J. Fluid Mech* 45, 513–520.
- Haile, E., Awgichew, G., 2019. Heat and mass transfer of magnetohydrodynamic nanofluid in a boundary layer with slip conditions along a permeable exponentially stretching sheet. *Journal of Nanofluids* 8, 1–12.
- Hoseinijad, F., Dinarvand, S., Yazdi, M.E., 2021. Manninen's mixture model for conjugate conduction and mixed convection heat transfer of a nanofluid in a rotational/stationary circular enclosure. *Int. J. Numer. Methods Heat Fluid Flow* 31 (5), 1662–1694.
- Jawad, M., Alam, M., Kirn Hameed, M., Akgül, A., 2024. Numerical simulation of Buongiorno's model on Maxwell nanofluid with heat and mass transfer using Arrhenius energy: a thermal engineering implementation. *J. Therm. Anal. Calorim.* 149, 5809–5822. <https://doi.org/10.1007/s10973-024-13133-4>.
- Khan, M., Irfan, M., Khan, W.A., 2019. Heat transfer enhancement for Maxwell nanofluid flow subject to convective heat transport. *Pramana. J. Phys* 92, 17.
- Khata, N.D., Kadim, Z.K., Khalaf, K.A., 2020. Numerical study of heat transfer enhancement in contour corrugated channel using water and engine oil. *CFD Lett.* 12, 17–23.
- Kodi, R., Ali, F., Khalid, M., Abdullaeva, B.S., Altijiri, R., Khan, M.I., 2023. Heat and mass transfer on MHD flow of Jeffrey nanofluid based on Cu and TiO₂ over an inclined plate and diffusion-thermo and radiation absorption effects. *Pramana* 97 (4), 202. <https://doi.org/10.1007/s12043-023-02673-3>.
- Kommaddi, H.B., Kodi, R., Ganteda, C., Lorenzini, G., 2023. Heat and mass transfer on unsteady MHD chemically reacting rotating flow of Jeffrey fluid past an inclined plate under the impact of hall current, diffusion thermo and radiation absorption. *J. Adv. Res. Fluid Mech. Therm. Sci.* 111 (2), 225–241. <https://doi.org/10.37934/arfmts.111.2.225241>.
- Kumar, S., Kumar, A.A., 2018. Comprehensive review on the heat transfer and nanofluid flow characteristics in different shaped channels. *Int. J. Ambient Energy* 32. <https://doi.org/10.1080/01430750.2018.1530139>.
- Mansourian, M., Dinarvand, S., Pop, I., 2022. Aqua cobalt ferrite/Mn-Zn ferrite hybrid nanofluid flow over a nonlinearly stretching permeable sheet in a porous medium. *J. Nanofluids* 11 (3), 383–391.
- Masuda, H., Ebata, A., Teramae, K., Hishinuma, N., 1993. Alteration of thermal conductivity and viscosity of liquid by dispersing ultra-fine particles. *NetsuBussei* 7, 227–233.
- Mohana Ramana, R., Maheswari, C., Mohiddin Shaw, S., Dharmiah, G., Fernandez-Gamiz, U., Noeiaghdam, S., 2024. Numerical investigation of 3-D rotating hybrid nanofluid Forchheimer flow with radiation absorption over a stretching sheet. *Results Eng.* 22, 102019. <https://doi.org/10.1016/j.rineng.2024.102019>.
- Nayak, M.K., Mahanta, G., Karmakar, K., Mohanty, P., Shaw, S., 2022. Effects of thermal radiation and stability analysis on MHD stagnation cassin fluid flow over the stretching surface with slip velocity. *AIP Conf. Proc.* 2435, 020045. <https://doi.org/10.1063/5.0084385>.
- Raju, A., Ojija, O., Kambhatla, P.K., 2020. A comparative study of heat transfer analysis on ethylene glycol or engine oil as base fluid with gold nanoparticle in presence of thermal radiation. *J. Term. Anal. Calorim.* 145, 2647–2660.
- Ramasekhar, G., Jawad, M., 2024. Characteristics of MWCNT, SWCNT, Cu and water based on magnetized flow of nanofluid with Soret and Dufour effects induced by moving wedge: consequence of Falkner-Skan power law. *Numer. Heat Transf., Part a: App.* 1–15. <https://doi.org/10.1080/10407782.2024.2341270>.
- Ramasekhar, G., Divya, A., Jakeer, S., Reddy, S.R.R., Algehyne, E.A., Jawad, M., Akgül, A., Hassani, M.K., 2024. Heat transfer innovation of engine oil conveying SWCNTs-MWCNTs-TiO₂ nanoparticles embedded in a porous stretching cylinder. *Sci Rep* 14, 16448. <https://doi.org/10.1038/s41598-024-65740-8>.
- Ramasekhar, G., Shaik, J., Reddisekhar Reddy, S.R., Divya, A., Jawad, M., Ali Yousif, B. A., 2024. Ali Yousif numerical investigation of cassin fluid flow performance of blood containing gold and Fe₃O₄ nanofluid injected into a stenotic artery. *Numer. Heat Transf., Part a: App.* 1–17. <https://doi.org/10.1080/10407782.2024.2372465>.
- Ravindranath Reddy, G., Ramakrishna Reddy, G., 2022. Casson nanofluid performance on MHD convective flow past a semi-infinite inclined permeable moving plate in presence of heat and mass transfer. *Heat Transf.* 1–21. <https://doi.org/10.1002/hjt.22645>.
- Sastry, D.R.V.S.R.K., Kumar, N.N., Kameswaran, P.K., Shaw, S., 2022. Unsteady 3D micropolar nanofluid flow through a squeezing channel: application to cardiovascular disorders. *Indian J. Phys.* 96, 57–70. <https://doi.org/10.1007/s12648-020-01951-9>.
- Shaw, S., Patra, A., Misra, A., Nayak, M.K., Chamkha, A.J., 2021. A numerical approach to the modeling of thomson and troian slip on nonlinear radiative microrotation of cassin nanomaterials in magnetohydrodynamics. *J. Nanofluids* 10, 305–315. <https://doi.org/10.1166/jon.2021.1790>.
- Shaw, S., Samantaray, S.S., Misra, A., Nayak, M.K., Makinde, O.D., 2022. Hydromagnetic flow and thermal interpretations of Cross hybrid nanofluid influenced by linear, nonlinear and quadratic thermal radiations for any Prandtl number. *Int. Commun. Heat Mass Transf.* 130, 105816. <https://doi.org/10.1016/j.icheatmasstransfer.2021.105816>.
- Sudhanshu, S.S., Sachin, S., Ashok, M., Manoj, K.N., Prakash, J., 2022. Darcy-Forchheimer up/downflow of entropy optimized radiative nanofluids with second-order slip, nonuniform source/sink, and shape effects. *Heat Transfer* 51 (3), 2318–2342. <https://doi.org/10.1002/hjt.22403>.
- Usman, M., Soomro, F.A., Haq, R.U.L., Wanga, W., Deftlerli, O., 2018. Thermal and velocity slip effects on Casson nanofluid flow over an inclined permeable stretching cylinder via collocation method. *Int. J. Heat Mass Transfer* 122, 1255–1263.
- Vasheghani, M.H., Marzbanrad, E., Zamani, C., Aminy, M., Raissi, B., 2013. Thermal conductivity and viscosity of TiO₂-engine oil nanofluids. *Int. J. Nanomech. Sci. Technol.* 4, 145–156.
- Waseem, M., Jawad, M., Naem, S., Majeed, A., 2024. Impact of motile microorganisms and chemical reaction on viscoelastic flow of non-newtonian fluid with thermal radiation subjected to exponentially stretching sheet amalgamated in darcy-forchheimer porous medium. *BioNanoSci.* 14, 1601–1612. <https://doi.org/10.1007/s12668-024-01435-8>.
- Zhang, L., Vaddemani, R.R., Ganjikutna, A., Bingi, S., Kodi, R., 2024. 3D-MHD mixed convection in a darcy-forchheimer maxwell fluid: Thermo diffusion, diffusion-thermo effects, and activation energy influence. *Case Studies Therm. Eng.* 61, 104916. <https://doi.org/10.1016/j.csite.2024.104916>.